Biomaterials 56 (2015) 26–35

Contents lists available at ScienceDirect

Biomaterials

journal homepage: www.elsevier.com/locate/biomaterials

Photothermal tumor ablation in mice with repeated therapy sessions using NIR-absorbing micellar hydrogels formed *in situ*

Chun-Wen Hsiao [a], Er-Yuan Chuang [a], Hsin-Lung Chen [a], Dehui Wan [b], Chiranjeevi Korupalli [a], Zi-Xian Liao [c], Ya-Ling Chiu [a], Wei-Tso Chia [d], Kun-Ju Lin [e, f, **], Hsing-Wen Sung [a, b, *]

[a] Department of Chemical Engineering, National Tsing Hua University, Hsinchu, Taiwan, ROC
[b] Institute of Biomedical Engineering, National Tsing Hua University, Hsinchu, Taiwan, ROC
[c] Institute of Medical Science and Technology, National Sun Yat-sen University, Kaohsiung, Taiwan, ROC
[d] Department of Orthopedics, National Taiwan University Hospital Hsinchu Branch, Hsinchu, Taiwan, ROC
[e] Healthy Aging Research Center, Department of Medical Imaging and Radiological Sciences, College of Medicine, Chang Gung University, Taoyuan, Taiwan, ROC
[f] Department of Nuclear Medicine and Molecular Imaging Center, Chang Gung Memorial Hospital, Taoyuan, Taiwan, ROC

ARTICLE INFO

Article history:
Received 13 December 2014
Received in revised form
28 March 2015
Accepted 29 March 2015
Available online 15 April 2015

Keywords:
Cancer therapy
Photothermal agent
pH-responsive micellar hydrogel
Multiple treatment sessions
Self-doped conducting polymer

ABSTRACT

Repeated cancer treatments are common, owing to the aggressive and resistant nature of tumors. This work presents a chitosan (CS) derivative that contains self-doped polyaniline (PANI) side chains, capable of self-assembling to form micelles and then transforming into hydrogels driven by a local change in pH. Analysis results of small-angle X-ray scattering indicate that the sol–gel transition of this CS derivative may provide the mechanical integrity to maintain its spatial stability in the microenvironment of solid tumors. The micelles formed in the CS hydrogel function as nanoscaled heating sources upon exposure to near-infrared light, thereby enabling the selective killing of cancer cells in a light-treated area. Additionally, photothermal efficacy of the micellar hydrogel is evaluated using a tumor-bearing mouse model; hollow gold nanospheres (HGNs) are used for comparison. Given the ability of the micellar hydrogel to provide spatial stability within a solid tumor, which prevents its leakage from the injection site, the therapeutic efficacy of this hydrogel, as a photothermal therapeutic agent for repeated treatments, exceeds that of nanosized HGNs. Results of this study demonstrate that this *in situ*-formed micellar hydrogel is a highly promising modality for repeated cancer treatments, providing a clinically viable, minimally invasive phototherapeutic option for therapeutic treatment.

1. Introduction

Cancer is one of the leading causes of death. Radiotherapy and chemotherapy are the most commonly used methods for treating cancer [1,2]. However, these treatments commonly cause systemic cytotoxicity owing to their non-specific drug delivery to all tissues, including healthy ones [3]. In recent years, minimally invasive approaches that use photothermal energy for the selective treatment of tumor cells have attracted much attention [4,5]. Photothermal therapy (PTT) has the advantage over radiotherapy and chemotherapy of having fewer side-effects [6].

PTT uses inorganic nanomaterials [7–9], organic dyes [10], or nanoparticles of conductive polymers (such as polyaniline, PANI) [11,12] that can strongly absorb near-infrared (NIR) laser light and effectively convert its light energy to localized heat for the photothermal ablation of tumor cells. However, these nanomaterials predominantly accumulate in the liver and spleen rather than the tumors when administered systematically [6,13,14]; additionally, they are typically nondegradable. Conversely, if implanted at the diseased site *via* local injection, most of these nanomaterials are susceptible to rapid clearance [15] because they are too small to be retained in the interstices of tissues [16,17]. These issues potentially

* Corresponding author. Department of Chemical Engineering, National Tsing Hua University, Hsinchu 30013, Taiwan, ROC. Tel.: +886 3 574 2504.
** Corresponding author. Healthy Aging Research Center, Department of Medical Imaging and Radiological Sciences, College of Medicine, Chang Gung University, Taoyuan, Taiwan, ROC.
E-mail addresses: kunjulin@gmail.com (K.-J. Lin), hwsung@mx.nthu.edu.tw (H.-W. Sung).

http://dx.doi.org/10.1016/j.biomaterials.2015.03.060
0142-9612/

limit the photothermal efficacy of these nanosized PTT agents in clinical applications.

Recently, we developed an *in situ*-formed hydrogel of a chitosan (CS) derivative that contained self-doped PANI side-chains [18]. The self-doped PANI in the hydrogel effectively converted NIR light energy into localized heat in a mouse model with subcutaneous abscesses, resulting in the thermal lysis of bacteria and reparation of the infected wound with a single photothermal treatment.

Clinically, the treatment of a cancer must commonly be repeated because cancers are both aggressive and resistant [19,20]. Owing to their rapid clearance *in vivo*, the aforementioned nanosized PTT agents may not be effective in repeated photothermal treatments. Therefore, a PTT material that can be retained at the diseased site and repeatedly activated by NIR light for localized tumor ablation is therefore urgently required.

This work further studies the feasibility of using the *in situ*-formed hydrogel of a CS derivative as an effective PTT agent in the repeated photothermal treatments of cancers. Hollow gold nanospheres (HGNs), an inorganic PTT agent [21–23], were used as a control. Fig. 1 schematically depicts the chemical structure of the synthesized CS derivative and the mechanism by which it photothermally treated Hep3B (a human hepatocellular carcinoma cell line) tumors that were created subcutaneously in a mouse model. The synthesized CS derivative was suspended in deionized (DI) water at pH 6.3 and injected intratumorally at the site of tumors to form hydrogels in a process that was driven by a local change in pH. The extracellular pH in the microenvironment of solid tumors is 6.9–7.0 [24,25]. Hydrogels are three-dimensional polymeric networks which provides themselves spatial stabilization, avoiding the leakage into the neighboring tissues. An 808 nm NIR laser beam was focused on the tumor for 5 min during each treatment session, and the tumor temperature was maintained at 50–55 °C. This process was repeated every four days for a total of four treatment sessions.

The sol–gel transition of the CS derivative in an aqueous medium that can provide spatial stability in the microenvironment of a solid tumor was investigated using small-angle X-ray scattering (SAXS). The fundamental material characteristics of the aqueous solution of the CS derivative, including its optical properties, photothermal effect and stability, and cytotoxicity were examined *in vitro*. The effectiveness of its photothermal ablation of Hep3B cells was investigated. Finally, the *in vivo* biocompatibility and special stability of the *in situ*-formed hydrogel, as well as its NIR-mediated therapeutic efficacy during repeated treatment sessions, were evaluated in mice.

2. Materials and methods

2.1. Materials

CS (viscosity 36 mPa s, 0.5% in 0.5% acetic acid at 20 °C) with approximately 85% deacetylation was purchased from Koyo Chemical Co. Ltd. (Tokyo, Japan). All other chemicals - aniline, ammonium persulfate (APS), hydrochloric acid (HCl), sodium hydroxide (NaOH), 1-methyl-2-pyrrolidinone (NMP), and 3-mercapto-1-propanesulfonic acid sodium salt (MPS-Na) - were obtained from Sigma–Aldrich (St Louis, MO, USA). Hep3B cells were obtained from the Bioresource Collection and Research Center, Food Industry Research and Development Institute, Hsinchu, Taiwan. Cell culture reagents were purchased from Invitrogen (Carlsbad, CA, USA).

2.2. Synthesis of test copolymers

PANI was grafted onto CS (*N*-PANI-grafted CS; NPA-CS) by the oxidative polymerization of aniline hydrochloride in the presence of APS and CS. Briefly, 2 g of CS was mixed with 900 mL of HCl (0.1 M). Following complete dissolution, aniline (14.5 mM) was added to the CS solution; then, an equimolar amount of APS was introduced into the mixed solution. The polymerization was performed for 3 h in an ice bath. The as-prepared copolymer (NPA-CS) was then neutralized and precipitated by NaOH; meanwhile, free PANI was removed using NMP. A concurrent reduction and substitution (CRS) method was then used to derivatize the grafted PANI with 0.1 M MPS-Na in an atmosphere of N_2 for 14 h, yielding the self-doped NMPA-CS [26]. The resultant NMPA-CS was precipitated by NaOH, purified with DI water, and then air-dried.

2.3. Sol–gel transition of aqueous NMPA-CS

Macroscopically, the aqueous solution of NMPA-CS thickened as its concentration was increased, forming an injectable viscous liquid at pH 6.3. When the pH reached 7.0, the solution underwent a dramatic physical transformation into a soft gel (insets in Fig. 2a), which was non-flowing. The effects of the environmental pH on the supramolecular structures of aqueous NMPA-CS (30 mg/mL) were examined by SAXS. Experiments were performed in the BL23A1 beamline at the National Synchrotron Radiation Research Center (NSRRC), Hsinchu, Taiwan. The obtained scattering intensity profile was a plot of scattering intensity $I(q)$ as a function of scattering vector, $q = (4\pi/\lambda)\sin(\theta/2)$ (θ = scattering angle), after corrections for

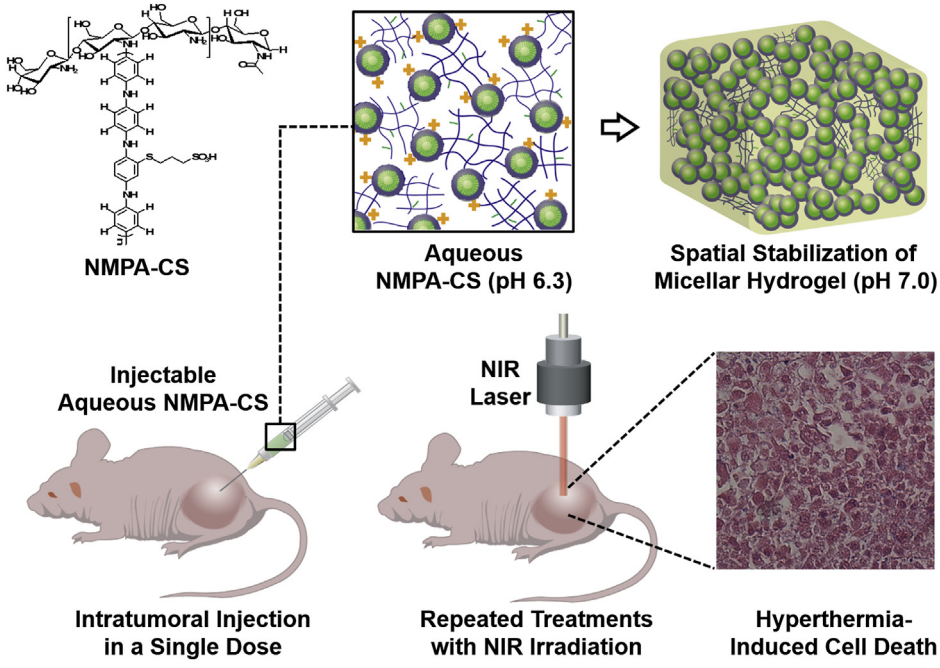

Fig. 1. Chemical structure of CS derivative that contained self-doped PANI side-chains and mechanism by which it photothermally treats tumors.

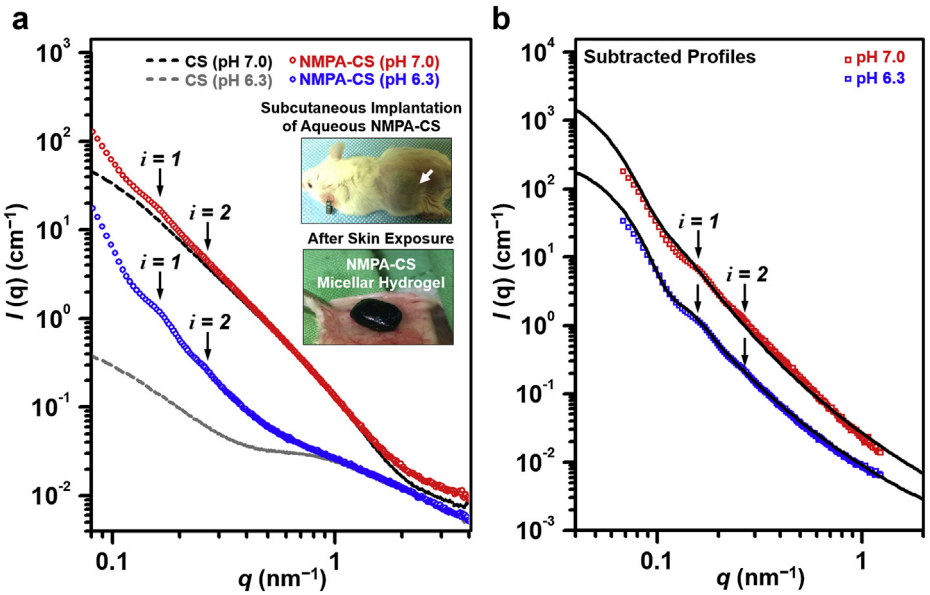

Fig. 2. (a) SAXS profiles of aqueous NMPA-CS and neat CS at pH 6.3 and 7.0, and (b) profiles obtained from subtracting one from the other and corresponding fitted results (black solid curves). Insets: photographs of a mouse model subcutaneously implanted with NMPA-CS micellar hydrogel before and after exposure of skin.

sample transmission, empty cell transmission, empty cell scattering, and the sensitivity of the detector [27].

The SAXS profile that was determined by the form factor of the micelles that were assembled by NMPA-CS was fitted using the core–shell sphere model, which considers the polydispersity of the core radius, given a size distribution that satisfies the Schultz distribution function [28]. Since both NMPA-CS micelles and free CS chains contributed to the SAXS profile of the experimentally obtained solution, the scattering that was caused by the micelles was obtained by subtracting the SAXS profile of neat CS from that of NMPA-CS with the application of an appropriate weighting factor.

2.4. Optical properties, photothermal effect and photostability of aqueous NMPA-CS

The UV–vis optical properties of an aqueous NMPA-CS solution with various pH values were studied using a SpectraMax M5 Microplate Reader (Molecular Devices, Sunnyvale, CA, USA). To elucidate its photothermal effect, an aqueous NMPA-CS solution (200 μg/mL) at pH 7.0 was exposed to an NIR laser (808 nm, Tanyu Tech., Taiwan) at a power density of 2 W/cm^2 for 5 min. The controls were aqueous solutions of CS (200 μg/mL), NPA-CS (200 μg/mL), and HGNs (15 μg/mL) at pH 7.0. The heat maps and temperature profiles of these solutions were recorded using an infrared (IR) thermal camera (ICI7320, Infrared Camera, Beaumont, TX, USA). To evaluate the photostability of NMPA-CS, the solution of NMPA-CS was irradiated with the aforementioned 808 laser for 5 min, and then naturally cooled to room temperature without laser illumination for 20 min. This cycle was performed ten times and temperature profiles of the NMPA-CS solution were recorded by the IR thermal camera.

2.5. Cytotoxicity of test samples

The *in vitro* cytotoxicity of NMPA-CS was qualitatively assessed using a Live/Dead staining method and quantitatively measured by the MTS assay. The untreated cells and cells co-incubated with CS or NPA-CS served as the controls. Hep3B cells (5×10^4 cells per well) were cultured in 48-well plates with the medium (pH 6.3) that contained 200 μg/mL of test samples for 24 h to evaluate their cytotoxicity.

2.6. In vitro photothermal ablation of tumor cells

Hep3B cells were cultivated in 48-well plates in the presence of NPA-CS or NMPA-CS (200 μg/mL). Following exposure to the NIR laser at a power density of 2 W/cm^2 for specified periods, cells in each plate were stained using the Live/Dead Viability Kit (Invitrogen) to differentiate the live from the dead cells. The results were photographed under a fluorescence microscope (Axio Observer Z1, Zeiss, Göttingen, Germany). The MTS assay was conducted to quantify the cell viability in the area that had been exposed to the laser light.

2.7. In vivo biocompatibility and spatial stability of NMPA-CS

Animals were care for and used in a manner consistent with the "Guide for the Care and Use of Laboratory Animals", prepared by the Institute of Laboratory Animal Resources, National Research Council and published by the National Academy Press. The protocol (#10258) was approved by the Institutional Animal Care and Use Committee of National Tsing Hua University at Hsinchu, Taiwan.

ICR mice (eight weeks old) were anesthetized using pentobarbital before the experiments were carried out. After the mice had been shaved and disinfected, 100 μL of the sterilized NMPA-CS solution (30 mg/mL) was subcutaneously injected into the right rear flank of each test mouse. At predetermined times, the mice were sacrificed, and the implanted NMPA-CS hydrogel along with its surrounding tissue were isolated and processed for histological (hematoxylin–eosin; H&E) and immunohistochemical analyses. In the immunohistochemical analysis, rat anti-mouse F4/80 antibody (MCA497GA; Serotec, Duesseldorf, Germany) was used to identify macrophages in the peri-implant tissue; nuclei were visualized by counterstaining with 4′,6′-diamidino-2-phenylindole (DAPI, Sigma–Aldrich). The stained sections were then examined under an inverted confocal laser scanning microscope (TCS SL, Leica, Germany).

2.8. In vivo photothermal therapy

A tumor-bearing mouse model, which was formed by the subcutaneous injection of Hep3B cells (5×10^6 cells in 100 μL Matrigel; BD Biosciences, Franklin Lakes, NJ) into the left flank region of athymic nude mice (BALB/cAnN.Cg-Foxn1nu/CrlNarl, 6–8 weeks old), was utilized to investigate the photothermal efficacy of the NMPA-CS hydrogel. When the tumors had grown to a mean volume of around 200 mm^3, the mice were divided into five groups and treated under one of the following five experimental conditions (n = 5 per group); no treatment (Control); exposed to laser alone (NIR); injected with NMPA-CS only (NMPA-CS); treated with HGNs and exposed to the laser (HGNs + NIR); and treated with NMPA-CS and exposed to the laser (NMPA-CS + NIR).

During each NIR treatment, mice were anesthetized and then exposed to the NIR laser (0.5 W/cm^2) for 5 min. This process was repeated every four days and a total of four treatment sessions were carried out. The tumor sizes and body weights of each test group were measured every other day and normalized to their initial values. Mice were humanely euthanized when the tumor size exceeded 3000 mm^3 [29].

At the end of the repeated treatments, the mice were made to fast overnight, anesthetized with isoflurane (2% in 100% O_2), and injected with 0.32 mCi ^{18}F-flourodeoxyglucose (^{18}F-FDG) in 100 μL of saline through the tail vein. A 10 min image acquisition was performed one hour following ^{18}F-FDG injection using a positron emission tomographic (PET) scanner (Inveon™, Siemens Medical Solutions, Knoxville, TN, USA). After the PET scan, whole-body computed tomographic (CT) images were acquired using NanoSPECT/CT (Bioscan, Washington, DC, USA) [30]. Finally, the mice were sacrificed, and the tumor tissues were retrieved and fixed in 4% neutral buffered formalin, embedded in paraffin, sectioned, and stained with H&E.

2.9. Statistical analysis

All results are presented as mean ± SD. The Student *t* test was used to compare the means of each pair of groups. Comparisons of more than two groups were made using one-way ANOVA followed by the Bonferroni post hoc test. Differences were regarded as statistically significant at $P < 0.05$.

3. Results and discussion

Recently, polymer solutions that can be transformed into hydrogels *in situ* as a result of changes in environmental stimuli have been extensively studied with a view to their use in the treatment of cancers [31–33]. The pH-sensitive polymer solution that was used in this work contained a CS derivative with self-doped PANI side-chains (NMPA-CS). The synthesized copolymers had been characterized in our previous publication [18].

3.1. pH-responsive sol–gel transition of aqueous NMPA-CS

Fig. 2a presents the SAXS profiles of aqueous NMPA-CS at pH 6.3 (blue curve) and pH 7.0 (red curve); the scattering profiles of neat CS at the corresponding pH values are also displayed (as the two dashed curves) for comparison. Both the liquid (pH 6.3) and gel (pH 7.0) forms of NMPA-CS yielded two peaks (marked by "$i = 1$" and "$i = 2$") of the form factor maxima of the supramolecular aggregates, which were generated by the hydrophobic interaction of the MPS-PNAI side-chains in NMPA-CS. Those form factor peaks clearly signaled that the aggregates had a relatively well-defined geometry. In contrast, the SAXS profiles of NMPA-CS in the high-q region ($q >$ *ca.* 1.0 and 0.6 nm^{-1} for pH 6.3 and 7.0, respectively) superposed well with those of neat CS, revealing free CS chains with a low degree of grafting of MPS-PANI.

The geometric characteristics of the supramolecular aggregates that were formed by NMPA-CS can be resolved by fitting the observed SAXS profiles using a plausible form factor model [28]. Prior to the fitting, the scattering curve associated only with the supramolecular aggregates was obtained by subtracting the SAXS profile of neat CS from that of NMPA-CS. Fig. 2b shows the resulting SAXS profiles at pH 6.3 and 7.0, which were fitted well using the core–shell sphere form factor, as revealed by the superposition of the solid curves on the experimental data, revealing a geometric characteristic of micelles.

Table 1 presents the structural parameters of the micelles (each with a core and shell that comprises MPS-PANI and CS chains, respectively) that were obtained by fitting. Since increasing the pH from 6.3 to 7.0 caused only a minor change in the micelle structure of NMPA-CS, the gelation of NMPA-CS that was triggered by this pH change is attributable to an immediate change in the spatial distribution of the micelles (rather than a large perturbation of the structure in the micelles), mediated by the free CS chains in the bulk solution. At lower pH (pH 6.3), at which degree of acidity the free CS chains are dissolved in the solution, the dispersion of the micelles was relatively uniform, so that the system behaved as a viscous liquid. Conversely, when the environmental pH was 7.0, the increased hydrophobicity of the shell regions (CS chains) induced micelle aggregation and the reduced solubility of the free CS chains in the bulk solution caused their significant aggregation, dramatically enhancing the scattering intensity (Fig. 2a, red curve). The micelles and the CS chains may have aggregated together, such that a fraction of the CS chains were located among the micelles, bridging or "gluing" them together, forming a three-dimensional aggregate of the micelles with long-range interconnectivity that constrained their mobility. The strong limitation of mobility was responsible for the gel property of the system.

Table 1
Structural parameters of core–shell spherical micelles formed by aqueous NMPA-CS, obtained by SAXS model fitting.

pH	$\langle R_{core} \rangle$ (nm)[a]	t_{shell} (nm)[b]	Polydispersity of core radius[c]
6.3	32.1	0.57	0.23
7.0	35.4	0.32	0.27

[a] Mean radius of core formed by MPS-PANI side-chains.
[b] Thickness of shell formed by CS backbone.
[c] Polydispersity of core, given as ratio of standard deviation of core radii to mean core radius.

The above results demonstrate that the micelles that are formed by NMPA-CS are important in the hydrogelation of aqueous NMPA-CS, which was driven by a change in environmental pH. The micellar hydrogel thus formed may exhibit spatial stabilization within a solid tumor for a prolonged period without leaking significantly into its surrounding healthy tissues. Additionally, the substituted MPS-PANI enables the micelles that are formed in the hydrogel to serve as nanoscaled heating sources when exposed to NIR light. These two unique features raise the possibility of using this micellar hydrogel system as an effective PTT material in the repeated treatments for photothermal tumor ablation.

3.2. Optical properties of aqueous NMPA-CS

PANI is one of the most well-known conducting polymers and has a range of biomedical applications [34–36]. Doping under strongly acidic conditions (pH 1.0) causes a red-shift of the main absorption peak of PANI to the NIR region, associating with charge transfer between its quinoid and benzenoid rings *via* increasing the efficiency of the movement of electrons [12]. In the NIR region, the absorption of light by tissue chromophores is relatively weak, allowing light of which wavelengths to penetrate the tissue deeply [37], making it useful as a "therapeutic window" for clinical applications. The absorption of NIR light by the doped form of PANI excites its electrons from the ground state to the excited state, subsequently relaxing through non-radiative transitions and then producing a considerable heat that can be utilized for cancer-cell ablation [11,12]. Nevertheless, as the pH increases above 4.0, PANI loses its NIR photothermal activity because of deprotonation (undoped form), which greatly limits the range of its clinical applications [38].

An effective approach to improving the pH-dependence of the photothermal activity of PANI involves conjugating MPS covalently on its backbone. This self-doped derivative (NMPA-CS) contains an ionizable, negatively charged functional group ($-SO_3^-$), which acts as an inner dopant anion, bound to the polymer backbone. The substitution reaction of MPS on the PANI side chains can occur only at the diiminoquinoid rings, which are uniformly separated by three diaminobenzenoid rings and account for around 25 mol % of the repeating unit of PANI (Fig. 3a) [26].

According to Fig. 3a, the UV–vis spectra of NPA-CS (the copolymer whose PANI side chains are not conjugated with MPS) varied markedly with its environmental pH. In a strongly acidic environment (pH 1.0), a polaron band appeared at 450 nm (indicated by the black arrow), a characteristic of the doped (conductive) form of PANI [39]; additionally, a strong absorption band was observed in the NIR region. However, in an environment with a high pH (pH 5.0 or 7.0), deprotonation of NPA-CS (undoped form) eliminated these bands. As presented in Fig. 3b, the change in the color of NPA-CS from green (doped form) to blue (undoped form) was caused by the disappearance of inter-bandgap states [40].

In contrast, NMPA-CS remained green even at higher pH values, because it contains self-doped PANI side chains. The self-doped NMPA-CS absorbed NIR absorbance in the physiological range of pH values much more strongly than did NPA-CS. However, the intensities of its optical-absorbance in the NIR region were significantly lower at higher pH values (pH 5.0 and 7.0) than at pH 1.0, probably because the NMPA-CS that was prepared herein had a self-doping degree much less than the optimal degree of doping [26].

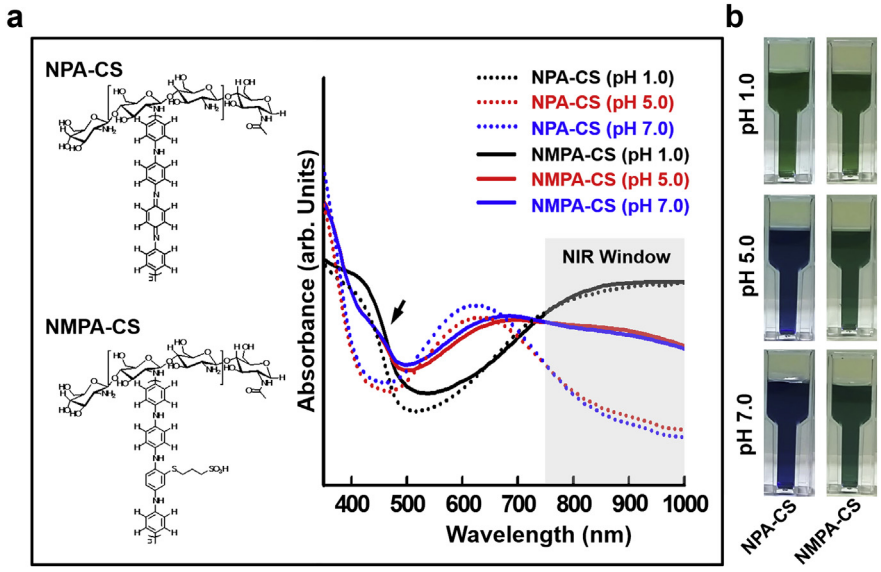

Fig. 3. (a) UV–vis absorbance spectra and (b) photographs of aqueous solutions of NPA-CS and NMPA-CS at various pH values.

3.3. Photothermal effect and photostability of aqueous NMPA-CS

In successful hyperthermic treatments, the tumor tissue must be heated to a minimum temperature for a minimum duration to cause cell death. Above 50 °C, the proteins in cells become denatured in 4–6 min, and their DNA is damaged, eventually causing cell death [41,42]. To confirm the NMPA-CS as a potential photothermal agent, an aqueous NMPA-CS solution (pH 7.0) was exposed to an 808 nm NIR laser at a power density of 2 W/cm^2 for 5 min, and the temperature profiles and heat maps were recorded using the IR thermal camera. Aqueous solutions of CS, NPA-CS, and HGNs at pH 7.0 were the controls. Exposing the aqueous CS solution to NIR light caused no significant temperature changes, while exposing NPA-CS resulted in a mild temperature increase to approximately 38 °C (Fig. 4a and b). The temperatures of aqueous solutions of NMPA-CS and HGNs both increased rapidly to about 54 °C within 5 min of exposure, owing to their much higher absorbance of NIR at physiological values of pH (Fig. 3a).

Multiple photothermal treatments are usually required to eradicate cancer cells [43,44]. Organic NIR dyes have exhibited less photostability than inorganic nanomaterials under prolonged light irradiation [10]. Therefore, the photostability of the NMPA-CS copolymer under repeated NIR light irradiations must be studied. In this study, an aqueous solution of NMPA-CS was illuminated by the NIR laser (2 W/cm^2) for 5 min, before being naturally cooled to room temperature, with the laser turned off, for 20 min; this cycle

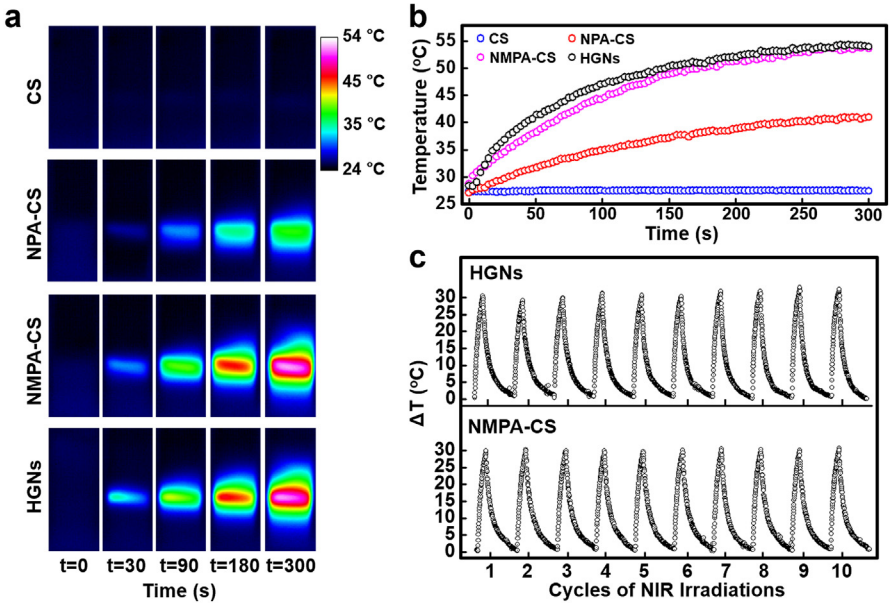

Fig. 4. (a) Thermographic images of aqueous solutions of CS, NPA-CS, NMPA-CS, and HGNs following exposure to an NIR laser (2.0 W/cm^2) and (b) Temperature evolution curves. (c) Elevated temperature profiles of aqueous HGNs and NMPA-CS over ten cycles of NIR exposure.

was conducted ten times. As presented in Fig. 4c, no significant change in the elevated temperature profiles was observed throughout the ten cycles of NIR light illumination, revealing the excellent photostability of NMPA-CS. Similar findings were also observed for HGNs. These experimental results suggest the potential of using this self-doped NMPA-CS as a PTT material for the photothermal ablation of cancer cells.

3.4. Cytotoxicity of NMPA-CS

An ideal photothermal agent should be nontoxic, and especially without non-specific biological toxicity [45]. Accordingly, the cytotoxicity of NMPA-CS must be quantified before its potential effectiveness in the photothermal killing of cancer cells can be explored. In the cytotoxicity study, Hep3B cells were cultured for 24 h in 48-well plates with a medium (pH 6.3) that contained NMPA-CS; controls were untreated cells and those incubated with CS or NPA-CS. During incubation, the pH value of the culture medium gradually recovered to the neutral pH of 7.0, under the influence of the bicarbonate/carbon dioxide buffering system, so test samples of CS, NPA-CS, and NMPA-CS progressively precipitated out as a result of the sensitivity of CS to pH, forming a layer on the top of the cultured cells (Fig. 5a). Their cytotoxicity was then evaluated qualitatively using a Live/Dead staining method and quantified by the MTS assay.

In the Live/Dead assay, the hydrolysis of calcein-AM in live cells produces green fluorescence, whereas ethidium homodimer is prevented from entering live cells and produces only red fluorescence in dead cells [27]. In contrast, the MTS assay measures the mitochondrial activity of live cells [46]. According to Fig. 5b, the test cells in each studied group emitted mostly green fluorescence, suggesting that treatment with test samples (CS, NPA-CS, or NMPA-CS) had a negligible effect on the viability of cells. Moreover, the total proportions of viable cells were comparable across all studied groups ($P > 0.05$), as determined by the measurements of optical density in the MTS assay (Fig. 5c). These analytical results indicate that no test samples exhibited significant toxicity.

3.5. In vitro photothermal ablation of cancer cells

The localized photothermal effects of NPA-CS and NMAP-CS on Hep3B cells were individually evaluated following exposure to the NIR laser (2 W/cm^2) for specified periods. Most cells in the group that had been treated with NPA-CS were stained with calcein-AM that fluoresces green following 5 min of exposure to NIR (Fig. 6a); additionally, the MTS assay revealed minimal changes in cell viability (Fig. 6b). These experimental results suggest that the heat that was generated by NPA-CS was insufficient to kill the treated cells, owing to its poor NIR absorbance at physiological pH values (Fig. 4b). In contrast, cells with red fluorescence in the group that received NMPA-CS were clearly observed at the spot that had been irradiated by the NIR laser. The diameter of this red-fluorescing area increased with the duration of exposure to the NIR light, reaching the width of the laser beam (approximately 4.9 mm) after 5 min of exposure (Fig. 6a); most or all of the cells in this zone were dead, as confirmed by the MTS assay ($P < 0.05$, Fig. 6b). This process occurred only upon photoactivation of NMPA-CS with the NIR laser, rendering it effective for the selective killing cancer cells in a light-treated area, potentially supporting therapies that pin-point a diseased site.

3.6. In vivo biocompatibility and spatial stability of NMPA-CS

The biocompatibility of a PTT agent must be properly characterized *in vivo* as an essential prerequisite for its clinical use. In a study of *in vivo* biocompatibility, an aqueous solution of NMPA-CS (30 mg/mL, 100 μL, pH 6.3) was directly injected through a needle into the subcutaneous space in ICR mice. A mouse model that is

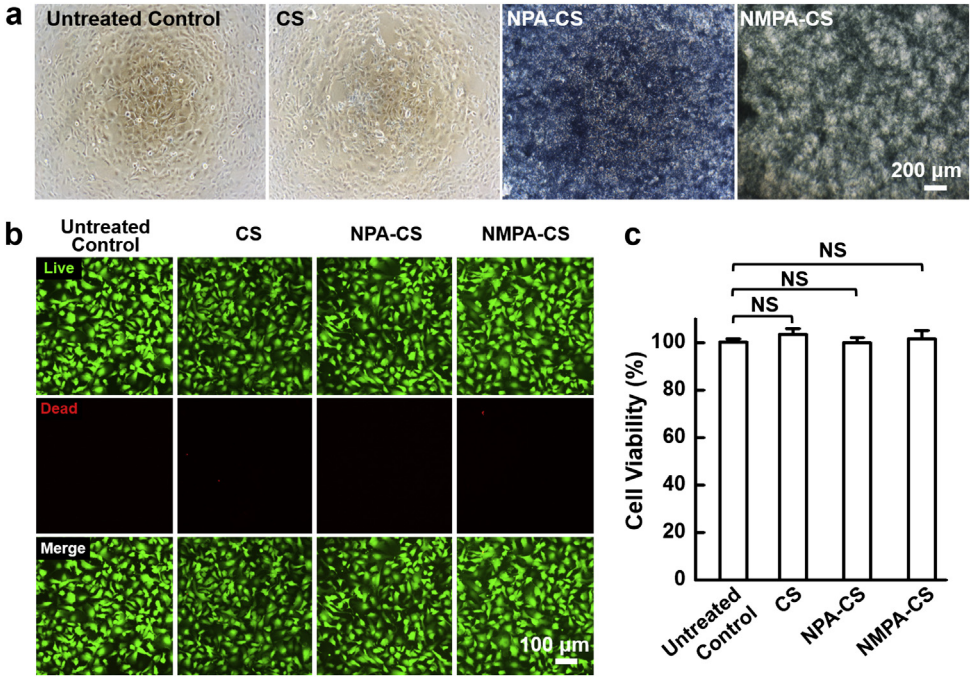

Fig. 5. (a) Photomicrographs of Hep3B cells following their co-incubation with CS, NPA-CS, or NMPA-CS for 24 h. Results concerning cytotoxicity: (b) qualitative results obtained using a Live/Dead staining method and (c) quantitative results obtained using MTS assay (n = 6). Live cells were stained green by calcein-AM and dead cells were stained red by ethidium homodimer. NS: not statistically significant. (For interpretation of the references to color in this figure legend, the reader is referred to the web version of this article.)

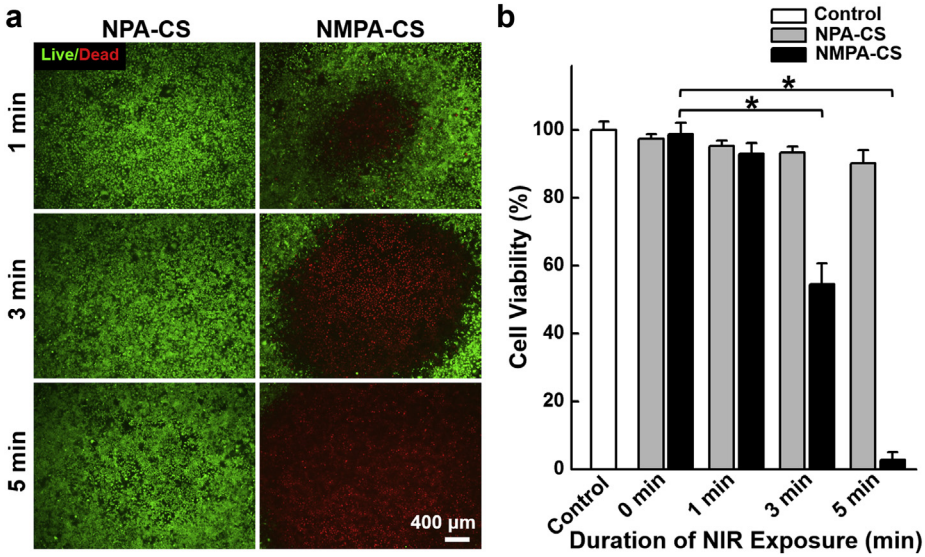

Fig. 6. Photothermal killing of Hep3B cells that were treated with NPA-CS or NMPA-CS and exposed to an NIR laser (2 W/cm^2) for specified periods: (a) images obtained following Live/Dead staining and (b) quantitative results concerning cell viability within area exposed to laser light, determined by MTS assay (n = 6). *Statistical significance at $P < 0.05$.

utilized in a biocompatibility study must be immunocompetent to enable any inflammatory responses to the grafted materials to be assessed [47]. At predetermined times, mice were sacrificed, and the implanted NMPA-CS hydrogel along with its surrounding tissue were then isolated and processed for histological examination.

Throughout the test period, the implanted NMPA-CS hydrogel did not cause an exaggerated inflammatory response. At two weeks post-implantation, activated fibroblasts with intermingling inflammatory cells dominated the peri-implant tissue response (Area 1 in Fig. 7a). Some inflammatory cells infiltrated the outer layer of the implanted hydrogel (as indicated by the white arrows in Area 1), while the main body of the hydrogel remained intact (Area 2). The peri-implant cells were identified by immunohistochemical staining using an F4/80 antibody, which can recognize the antigen that is expressed by macrophages [48]. The stained sections were also counterstained with DAPI to mark the cell nuclei. According to Fig. 7b, F4/80-positive cells (macrophages) were observed in the vicinity of the implanted hydrogel.

After week six, the implanted hydrogel was still present at the original site of implantation, verifying its spatial stability. The density of inflammatory cells in the peri-implant tissue (Area 3) that was in direct contact with the NMPA-CS hydrogel was reduced. By this time, fibroblasts and inflammatory cells had already migrated into the implanted hydrogel and some degree of

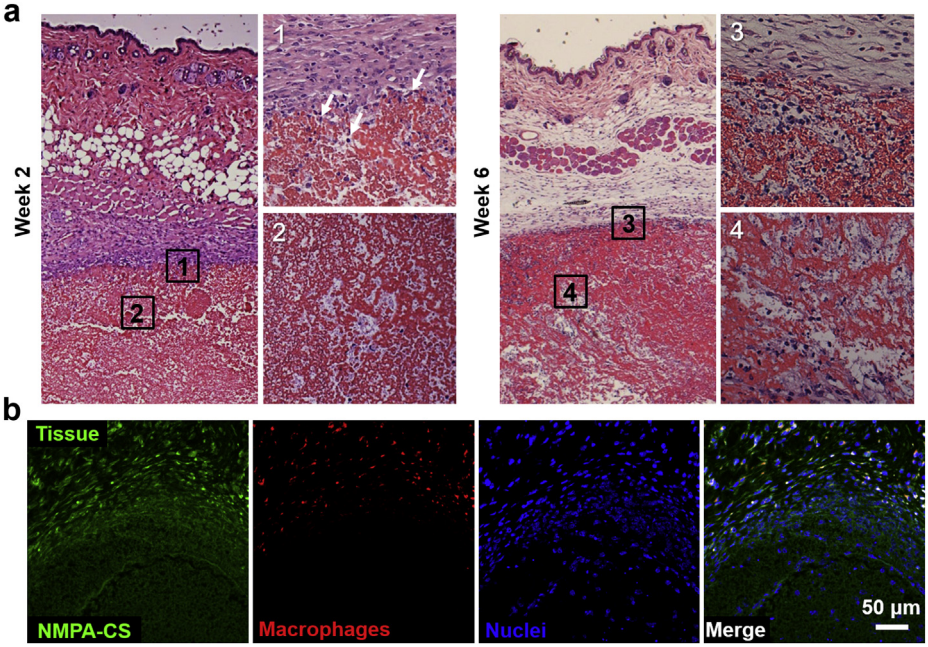

Fig. 7. (a) Histological photomicrographs of NMPA-CS micellar hydrogel and surrounding tissue that were retrieved at two and six weeks after implantation. (b) Results of immunohistochemical staining of peri-implant tissue; green color was observed as a result of autofluorescence of tissue section. (For interpretation of the references to color in this figure legend, the reader is referred to the web version of this article.)

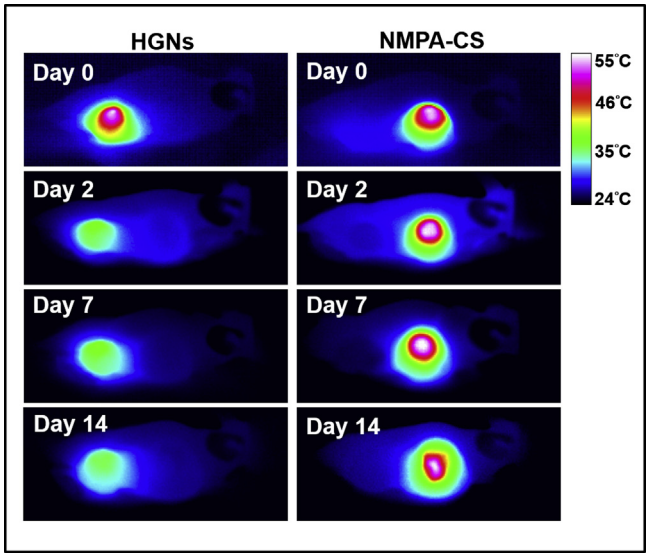

Fig. 8. Thermographic images of Hep3B tumor-bearing mice that were intratumorally injected with single dose of NMPA-CS or HGNs following exposure to an NIR laser (0.5 W/cm^2, 5 min), taken at specified times.

degradation of the hydrogel was observed (Area 4). Overall, the implanted NMPA-CS hydrogel provoked a mild foreign-body reaction with slow degradation. The presence of macrophages might have been responsible for the phagocytosis of the polymer and its degradation *in vivo* [27].

3.7. *In vivo* photothermal therapy

Although cell destruction is usually apparent following a single photothermal treatment, the recurrence of tumors, which is associated with a negative effect on long-term survival, calls into question the efficacy of such treatment, suggesting that it should be applied repeatedly [43]. To conduct repeated photothermal treatments, the administered PTT agent must be concentrated in the selected tumor tissue and remain there for long enough to be activated by the laser. In this study, BALB/c nude mice with subcutaneous Hep3B tumors were utilized to evaluate the spatial stability of aqueous NMPA-CS (30 mg/mL, 100 μL) following its intratumoral injection. These nude mice were immunocompromised and did not reject human tumor grafts [49]. The HGNs (60 μg/mL, 100 μL) were the control. The tumors were then individually and repeatedly exposed to NIR (0.5 W/cm^2) for 5 min at specified intervals, and the local temperatures were recorded using the IR thermal camera.

Immediately following injection with NMPA-CS or HGNs (day 0), the temperatures of the tumors in both studied groups increased rapidly to 50–55 °C (Fig. 8), because of their excellent NIR absorbance. After repeated treatments within two weeks, the tumor containing HGNs showed a temperature decrease, whereas the one with NMPA-CS maintained approximately the same temperature, probably because the tumor tissue was highly permeable to the nanosized HGNs, so as time passed, a significant fraction of the implanted HGNs leaked out through the hole that was made by the puncturing needle, or they spread to the adjacent tissues, significantly reducing their photothermal ability. Conversely, an *in situ*-formed micellar hydrogel that could provide spatial stabilization prevented the leakage of NMPA-CS from the injection site following intratumoral injection, preserving its activity for repeatable photothermal therapy.

In repeated NIR treatments, the *in vivo* efficacy of the NMPA–CS–induced photothermal ablation of cancer cells was studied in a Hep3B tumor model in nude mice. During each photothermal treatment, mice were anesthetized and then exposed to the 808 nm laser (0.5 W/cm^2) for 5 min. This process was repeated every four days for a total of four treatment sessions.

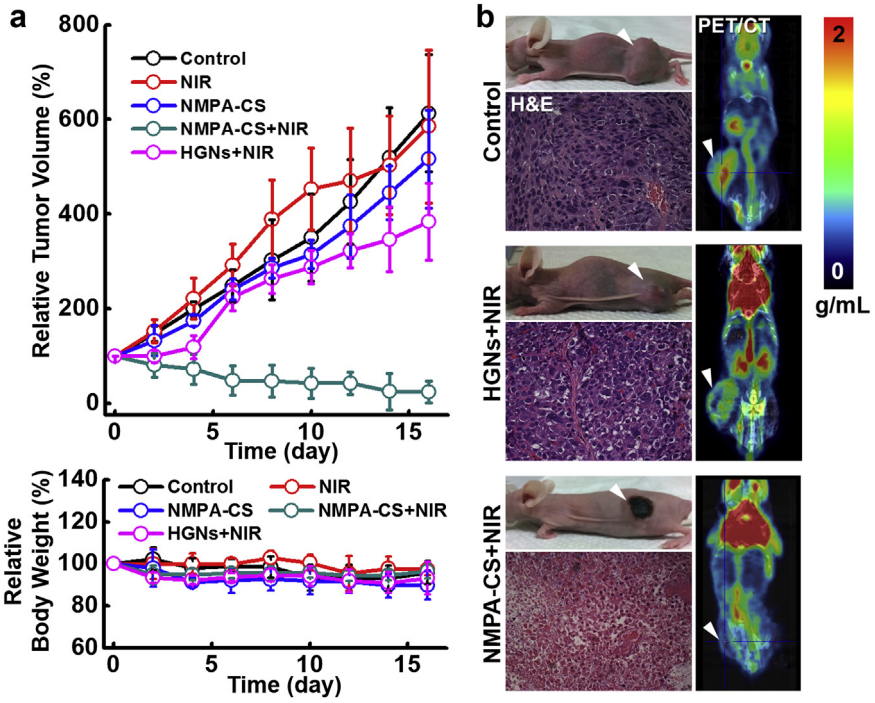

Fig. 9. (a) Changes in relative tumor volume and body weight of mice with Hep3B tumors upon various treatments (n = 5). (b) Photographs, histological photomicrographs, and ^{18}F-FDG PET/CT co-registered images of untreated control group and groups treated with HGNs + NIR or NMPA-CS + NIR.

According to Fig. 9a, neither the laser irradiation alone (NIR) nor NMPA-CS injection alone (NMPA-CS) affected the tumor growth relative to that of the untreated control (Control, $P > 0.05$). On the other hand, the mice that received HGNs and were exposed to the NIR laser (HGNs + NIR) exhibited clearly suppressed tumor growth following the first NIR treatment; however, the growth of tumor proceeded thereafter, probably owing to the leakage of HGNs from the injection site of the tumor. In marked contrast, the mice that were treated with NMPA-CS + NIR demonstrated effectively suppressed tumor growth and continued to show no sign of tumor progression for the duration of the study, and only black scars on the skin were present at the tumor site (Fig. 9b). This encouraging result is attributed to the spatial stability of the NMPA-CS micellar hydrogel within the tumor, which allows repeated photothermal treatments.

^{18}F-FDG has been widely used as a PET agent in tumor examinations [50]. Increased FDG uptake normally reflects the high proliferative activity of tumor tissues, and so assists in predicting the therapeutic efficacy of the corresponding treatment. In this work, at the end of repeated treatments, the efficacy of the photothermal ablation of the tumor that had been treated with NMPA-CS + NIR was further examined using a PET scanner and by histological analyses of tumor sections that had been stained with H&E. According to Fig. 9b, the uptake of FDG in the group that received NMPA-CS + NIR was remarkably lower than that in the untreated control group or the group that was treated with HGNs + NIR. Additionally, signs of significant cell destruction were noted only in the group that had been photothermally treated with NMPA-CS + NIR and not in the group that received HGNs. These analytical data demonstrate that the therapeutic efficacy of NMPA-CS micellar hydrogel as a PTT agent in repeated treatments exceeds that of nanosized HGNs.

The toxic side-effects of the photothermal treatment of NMPA-CS were evaluated by quantifying variations in body weight, which reflect the general toxicity of the treatment modality [51]. According to Fig. 9a, no significant changes in body weight of the tumor-bearing mice occurred throughout the study period, suggesting no apparent toxic side-effects of the photothermal treatment of NMPA-CS.

4. Conclusions

The NMPA-CS micellar hydrogel formed herein can successfully and repeatedly convert NIR light into localized heat, and provides the PTT agent sufficient mechanical integrity to retain spatial stability *in situ* for a prolonged period. The animal study reveals the excellent tumor treatment efficacy of NMPA-CS micellar hydrogel without any significant toxic side-effects after multiple treatment sessions. This investigation establishes the feasibility of using the *in situ*-formed micellar hydrogel as a safe, repeatedly applicable and minimally invasive system for the photothermal ablation of tumors.

Acknowledgments

This work was supported by a grant from the National Science Council (NSC 103-2221-E-007-022-MY3), Taiwan (ROC). The PET-imaging study was supported by grants from Chang Gung Memorial Hospital at Linkou (CMRPG300161 and CMRPG391513), Taiwan.

References

[1] Baskar R, Lee KA, Yeo R, Yeoh KW. Cancer and radiation therapy: current advances and future directions. Int J Med Sci 2012;9:193–9.
[2] DeVita Jr VT, Chu E. A history of cancer chemotherapy. Cancer Res 2008;68:8643–53.
[3] Thakor AS, Gambhir SS. Nanooncology: the future of cancer diagnosis and therapy. CA Cancer J Clin 2013;63:395–418.
[4] Chen Q, Liang C, Wang X, He J, Li Y, Liu Z. An albumin-based theranostic nano-agent for dual-modal imaging guided photothermal therapy to inhibit lymphatic metastasis of cancer post surgery. Biomaterials 2014;35:9355–62.
[5] Dickerson EB, Dreaden EC, Huang X, El-Sayed IH, Chu H, Pushpanketh S, et al. Gold nanorod assisted near-infrared plasmonic photothermal therapy (PPTT) of squamous cell carcinoma in mice. Cancer Lett 2008;269:57–66.
[6] Cheng M, Wang H, Zhang Z, Li N, Fang X, Xu S. Gold nanorod-embedded electrospun fibrous membrane as a photothermal therapy platform. ACS Appl Mater Interfaces 2014;6:1569–75.
[7] Liu H, Chen D, Li L, Liu T, Tan L, Wu X, et al. Multifunctional gold nanoshells on silica nanorattles: a platform for the combination of photothermal therapy and chemotherapy with low systemic toxicity. Angew Chem Int Ed 2011;50:891–5.
[8] Liu Z, Cheng L, Zhang L, Yang Z, Liu Z, Fang J. Sub-100 nm hollow Au–Ag alloy urchin-shaped nanostructure with ultrahigh density of nanotips for photothermal cancer therapy. Biomaterials 2014;35:4099–107.
[9] Cheng L, Gong H, Zhu W, Liu J, Wang X, Liu G, et al. PEGylated Prussian blue nanocubes as a theranostic agent for simultaneous cancer imaging and photothermal therapy. Biomaterials 2014. http://dx.doi.org/10.1016/j.biomaterials.2014.09.004. Available from: http://www.sciencedirect.com/science/article/pii/. S0142961214009892.
[10] Lim CK, Shin J, Lee YD, Kim J, Oh KS, Yuk SH, et al. Phthalocyanine-aggregated polymeric nanoparticles as tumor-homing near-infrared absorbers for photothermal therapy of cancer. Theranostics 2012;2:871–9.
[11] Zhou J, Lu ZG, Zhu XJ, Wang XJ, Liao Y, Ma ZF, et al. NIR photothermal therapy using polyaniline nanoparticles. Biomaterials 2013;34:9584–92.
[12] Yang J, Choi J, Bang D, Kim E, Lim EK, Park H, et al. Convertible organic nanoparticles for near-infrared photothermal ablation of cancer cells. Angew Chem Int Ed 2011;50:441–4.
[13] De Jong WH, Hagens WI, Krystek P, Burger MC, Sips AJ, Geertsma RE. Particle size-dependent organ distribution of gold nanoparticles after intravenous administration. Biomaterials 2008;29:1912–9.
[14] Riviere JE. Pharmacokinetics of nanomaterials: an overview of carbon nanotubes, fullerenes and quantum dots. Wiley Interdiscip Rev Nanomed Nanobiotechnol 2009;1:26–34.
[15] Geng Y, Dalhaimer P, Cai S, Tsai R, Tewari M, Minko T, et al. Shape effects of filaments versus spherical particles in flow and drug delivery. Nat Nanotechnol 2007;2:249–55.
[16] Huang X, Li L, Liu T, Hao N, Liu H, Chen D, et al. The shape effect of mesoporous silica nanoparticles on biodistribution, clearance, and biocompatibility in vivo. ACS Nano 2011;5:5390–9.
[17] Sykes EA, Chen J, Zheng G, Chan WC. Investigating the impact of nanoparticle size on active and passive tumor targeting efficiency. ACS Nano 2014;8:5696–706.
[18] Hsiao CW, Chen HL, Liao ZX, Sureshbabu R, Hsiao HC, Lin SJ, et al. Effective photothermal killing of pathogenic bacteria by using spatial tunable colloidal gels with nano-localized heating sources. Adv Funct Mater 2015;25:721–8.
[19] Master A, Malamas A, Solanki R, Clausen DM, Eiseman JL, Sen Gupta A. A cell-targeted photodynamic nanomedicine strategy for head and neck cancers. Mol Pharm 2013;10:1988–97.
[20] Kitamoto M, Imagawa M, Yamada H, Watanabe C, Sumioka M, Satoh O, et al. Radiofrequency ablation in the treatment of small hepatocellular carcinomas: comparison of the radiofrequency effect with and without chemoembolization. Am J Roentgenol 2003;181:997–1003.
[21] Vankayala R, Lin C-C, Kalluru P, Chiang C-S, Hwang KC. Gold nanoshells-mediated bimodal photodynamic and photothermal cancer treatment using ultra-low doses of near infra-red light. Biomaterials 2014;35:5527–38.
[22] Lu W, Melancon MP, Xiong C, Huang Q, Elliott A, Song S, et al. Effects of photoacoustic imaging and photothermal ablation therapy mediated by targeted hollow gold nanospheres in an orthotopic mouse xenograft model of glioma. Cancer Res 2011;71:6116–21.
[23] Wan DH, Chen HL, Lin YS, Chuang SY, Shieh J, Chen SH. Using spectroscopic ellipsometry to characterize and apply the optical constants of hollow gold nanoparticles. ACS Nano 2009;3:960–70.
[24] Wong P, Lee C, Tannock IF. Reduction of intracellular pH as a strategy to enhance the pH-dependent cytotoxic effects of melphalan for human breast cancer cells. Clin Cancer Res 2005;11:3553–7.
[25] Tannock IF, Rotin D. Acid pH in tumors and its potential for therapeutic exploitation. Cancer Res 1989;49:4373–84.
[26] Han CC, Lu CH, Hong SP, Yang KF. Highly conductive and thermally stable self-doping propylthiosulfonated polyanilines. Macromolecules 2003;36:7908–15.
[27] Chiu YL, Chen SC, Su CJ, Hsiao CW, Chen YM, Chen HL, et al. pH-triggered injectable hydrogels prepared from aqueous *N*-palmitoyl chitosan: in vitro characteristics and in vivo biocompatibility. Biomaterials 2009;30:4877–88.
[28] Feigin LA, Svergun DI. Structure analysis by small-angle X-ray and neutron scattering. New York: Plenum Press; 1987.
[29] Herr I, Ucur E, Herzer K, Okouoyo S, Ridder R, Krammer PH, et al. Glucocorticoid cotreatment induces apoptosis resistance toward cancer therapy in carcinomas. Cancer Res 2003;63:3112–20.
[30] Yeh CN, Lin KJ, Hsiao IT, Yen TC, Chen TW, Jan YY, et al. Animal PET for thioacetamide-induced rat cholangiocarcinoma: a novel and reliable platform. Mol Imaging Biol 2008;10:209–16.

[31] Ta HT, Dass CR, Dunstan DE. Injectable chitosan hydrogels for localised cancer therapy. J Control Release 2008;126:205–16.
[32] Azhdarinia A, Yang DJ, Yu DF, Mendez R, Oh C, Kohanim S, et al. Regional radiochemotherapy using in situ hydrogel. Pharm Res 2005;22:776–83.
[33] Cheng Y, He C, Ding J, Xiao C, Zhuang X, Chen X. Thermosensitive hydrogels based on polypeptides for localized and sustained delivery of anticancer drugs. Biomaterials 2013;34:10338–47.
[34] Qazi TH, Rai R, Boccaccini AR. Tissue engineering of electrically responsive tissues using polyaniline based polymers: a review. Biomaterials 2014;35:9068–86.
[35] Thrivikraman G, Madras G, Basu B. Intermittent electrical stimuli for guidance of human mesenchymal stem cell lineage commitment towards neural-like cells on electroconductive substrates. Biomaterials 2014;35:6219–35.
[36] Hsiao CW, Bai MY, Chang Y, Chung MF, Lee TY, Wu CT, et al. Electrical coupling of isolated cardiomyocyte clusters grown on aligned conductive nanofibrous meshes for their synchronized beating. Biomaterials 2013;34:1063–72.
[37] Wang M, Mi CC, Wang WX, Liu CH, Wu YF, Xu ZR, et al. Immunolabeling and NIR-excited fluorescent imaging of HeLa cells by using $NaYF_4$:Yb,Er upconversion nanoparticles. ACS Nano 2009;3:1580–6.
[38] Mu SL. Nanostructured polyaniline synthesized using interface polymerization and its redox activity in a wide pH range. Synth Met 2010;160:1931–7.
[39] Ozkazanc E, Zor S, Ozkazanc H, Guney HY, Abaci U. Synthesis, characterization and dielectric behavior of (ES)-form polyaniline/cerium(III)-nitrate-hexahydrate composites. Mater Chem Phys 2012;133:356–62.
[40] Park J, Bang D, Jang K, Haam S, Yang J, Na S. The work function of doped polyaniline nanoparticles observed by Kelvin probe force microscopy. Nanotechnology 2012;23:365705–11.
[41] Vankayala R, Huang YK, Kalluru P, Chiang CS, Hwang KC. First demonstration of gold nanorods-mediated photodynamic therapeutic destruction of tumors via near infra-red light activation. Small 2014;10:1612–22.
[42] del Real RP, Arcos D, Vallet-Regi M. Implantable magnetic glass-ceramic based on (Fe,Ca)SiO_3 solid solutions. Chem Mater 2002;14:64–70.
[43] Chen WR, Adams RL, Higgins AK, Bartels KE, Nordquist RE. Photothermal effects on murine mammary tumors using indocyanine green and an 808-nm diode laser: an in vivo efficacy study. Cancer Lett 1996;98:169–73.
[44] Tsai MF, Chang SHG, Cheng FY, Shanmugam V, Cheng YS, Su CH, et al. Au nanorod design as light-absorber in the first and second biological near-infrared windows for in vivo photothermal therapy. ACS Nano 2013;7:5330–42.
[45] Zha ZB, Wang JR, Qu EZ, Zhang SH, Jin YS, Wang SM, et al. Polypyrrole hollow microspheres as echogenic photothermal agent for ultrasound imaging guided tumor ablation. Sci Rep-UK 2013;3:2360–8.
[46] Malich G, Markovic B, Winder C. The sensitivity and specificity of the MTS tetrazolium assay for detecting the in vitro cytotoxicity of 20 chemicals using human cell lines. Toxicology 1997;124:179–92.
[47] Chang J, Gupta G. Tissue engineering for the hand: research advances and clinical applications. New Jersey: World Scientific; 2010.
[48] Schaller E, Macfarlane AJ, Rupec RA, Gordon S, McKnight AJ, Pfeffer K. Inactivation of the F4/80 glycoprotein in the mouse germ line. Mol Cell Biol 2002;22:8035–43.
[49] Richmond A, Su YJ. Mouse xenograft models vs GEM models for human cancer therapeutics. Dis Model Mech 2008;1:78–82.
[50] Boellaard R, O'Doherty MJ, Weber WA, Mottaghy FM, Lonsdale MN, Stroobants SG, et al. FDG PET and PET/CT: EANM procedure guidelines for tumour PET imaging: version 1.0. Eur J Nucl Med Mol Imaging 2010;37:181–200.
[51] Chen KJ, Chaung EY, Wey SP, Lin KJ, Cheng F, Lin CC, et al. Hyperthermia-mediated local drug delivery by a bubble-generating liposomal system for tumor-specific chemotherapy. ACS Nano 2014;8:5105–15.